



Identification of GPI-anchored protein LYPD1 as an essential factor for odontoblast differentiation in tooth development

Received for publication, October 25, 2022, and in revised form, February 19, 2023. Published, Papers in Press, March 23, 2023.
<https://doi.org/10.1016/j.jbc.2023.104638>

Yao Fu^{1,‡}, Kanako Miyazaki^{1,‡}, Yuta Chiba^{2,3}, Keita Funada¹, Tomomi Yuta¹, Tian Tian¹, Kanji Mizuta¹,
Jumpei Kawahara¹, Ling Zhang¹, Daniel Martin⁴, Tsutomu Iwamoto⁵, Ichiro Takahashi¹,
Satoshi Fukumoto^{2,3,6,*}, and Keigo Yoshizaki^{1,2,*}

From the ¹Section of Orthodontics and Dentofacial Orthopedics, Division of Oral Health, Growth and Development, ²Dentocraniofacial Development and Regeneration Research Center, and ³Section of Pediatric Dentistry, Division of Oral Health, Growth and Development, Kyushu University Faculty of Dental Science, Fukuoka, Japan; ⁴Genomics and Computational Biology Core (National Institute on Deafness and Other Communication Disorders), National Institutes of Health, Bethesda, Maryland, USA; ⁵Division of Oral Health Sciences, Department of Pediatric Dentistry/Special Needs Dentistry, Graduate School of Medical and Dental Sciences, Tokyo Medical and Dental University, Tokyo, Japan; ⁶Division of Pediatric Dentistry, Department of Community Social Dentistry, Tohoku University Graduate School of Dentistry, Sendai, Japan

Reviewed by members of the JBC Editorial Board. Edited by Phillip A. Cole

Lipid rafts are membrane microdomains rich in cholesterol, sphingolipids, glycosylphosphatidylinositol-anchored proteins (GPI-APs), and receptors. These lipid raft components are localized at the plasma membrane and are essential for signal transmission and organogenesis. However, few reports have been published on the specific effects of lipid rafts on tooth development. Using microarray and single-cell RNA sequencing methods, we found that a GPI-AP, lymphocyte antigen-6/Plaur domain-containing 1 (*Lypd1*), was specifically expressed in preodontoblasts. Depletion of *Lypd1* in tooth germ using an *ex vivo* organ culture system and in mouse dental pulp (mDP) cells resulted in the inhibition of odontoblast differentiation. Activation of bone morphogenetic protein (BMP) signaling by BMP2 treatment in mDP cells promoted odontoblast differentiation *via* phosphorylation of Smad1/5/8, while this BMP2-mediated odontoblast differentiation was inhibited by depletion of *Lypd1*. Furthermore, we created a deletion construct of the C terminus containing the omega site in LYPD1; this site is necessary for localizing GPI-APs to the plasma membrane and lipid rafts. We identified that this site is essential for odontoblast differentiation and morphological change of mDP cells. These findings demonstrated that LYPD1 is a novel marker of preodontoblasts in the developing tooth; in addition, they suggest that LYPD1 is important for tooth development and that it plays a pivotal role in odontoblast differentiation by regulating Smad1/5/8 phosphorylation through its effect as a GPI-AP in lipid rafts.

Heterogeneous cell membranes contain transient and dynamic domains with varying characteristics, the most prominent of which are organized lipid-driving domains called lipid rafts (1). Lipid rafts are microdomains rich in cholesterol,

sphingolipids, glycosylphosphatidylinositol-anchored proteins (GPI-APs), and receptors (2). Although rafts float freely in the liquid-disordered bilayer of the cell membrane, once they are activated, they aggregate into larger platforms and recruit selective lipids and proteins to perform pathophysiological roles, including membrane transport, signaling, cell adhesion, migration, or apoptosis (3, 4). Previous studies have shown that lipid rafts and their components are essential for neuronal differentiation of different types of stem cells, including human dental pulp stem cells (5, 6). Sphingomyelin phosphodiesterase 3 (*Smpd3*), a membrane-bound enzyme that hydrolyzes sphingomyelin in lipid rafts to modulate lipid-raft integrity, has been implicated in dentinogenesis imperfecta and has been shown to be localized in odontoblasts (7, 8). Furthermore, growth arrest-specific 1 (*Gas1*) is known as a GPI-anchored membrane protein, and it has been reported that mice engineered with *Gas1* loss-of-function mutation and human subjects with pathogenic mutations in *GAS1* exhibit defective coronal morphology and reduced coronal dimensions in the molar dentition (9). Thus, lipid rafts play a crucial role in tooth development. GPI-APs are widely present among all eukaryotic organisms; they have been identified in at least 150 human proteins (10). Although protein molecules bound to GPI anchors have no common characteristics, they are associated with membrane microdomains or membrane rafts through GPI-dependent membrane anchoring (10). Their partitioning within the raft is considered to trigger activation cascades; therefore, these GPI-APs are often used as models for studying signaling “platforms,” the aggregation of signaling molecules induced by stimulation (11). Although there is persistent research focus on GPI-APs, few studies have evaluated their involvement in tooth development.

Tooth morphogenesis requires mutual induction of epithelial and mesenchymal cells, which originate from the ectoderm and neural crest-derived mesenchyme, respectively. In mice, the dental papilla is a condensation of ectomesenchymal cells partially encapsulated by epithelial cells that

[‡] These authors contributed equally to this work.

* For correspondence: Satoshi Fukumoto, fukumoto@dent.kyushu-u.ac.jp;
Keigo Yoshizaki, yosizaki@dent.kyushu-u.ac.jp.

***LYPD1* regulates odontoblast differentiation**

forms at the cap stage (embryonic day [E] 14). In the subsequent bell stage (E16), the dental papilla cells (DPCs) underlying the epithelium differentiate into preodontoblasts and odontoblasts, eventually secreting the dentin matrix (12). The dental follicle is the condensed dental mesenchyme with more peripheral cells extending around the epithelial dental component that develops into osteoblasts, cementoblasts, and fibroblasts (12). Although the dental papilla and dental follicle are derived from dental mesenchymal cells, they have different cellular differentiation fates. We hypothesized that specific genes determine the direction of their differentiation. Classical reconstitution experiments have demonstrated that dental epithelium cells exhibit odontogenic potential before the bud stage (13). However, as tooth development proceeds to the cap and bell stages, this capability to induce tooth formation shifts to DPCs, which subsequently direct the formation of the tooth and its final shape (14). For elucidating the mechanism of tooth development, a better understanding is required regarding the differentiation of DPCs to odontoblasts.

In this study, we aimed to screen tooth-specific GPI-APs using a combination of microarray and single-cell RNA sequencing (scRNA-seq) methods and identified the role of the preodontoblast-specific GPI-AP *LYPD1* in the developing tooth. Here, we demonstrate the mechanism underlying the function of *LYPD1* during odontoblast differentiation.

Results

***Lypd1* is highly expressed in the dental mesenchyme during tooth development**

To identify the genes specifically expressed in the dental papilla that are essential for odontoblast differentiation, we conducted microarray analysis of E14 mouse molar dental papilla (Fig. 1A). We dissected the dental papilla and dental follicle from E14 mouse molars and compared the gene expression by scatter plot analysis (Fig. 1B and Table S1). From the microarray analysis, we found that the GPI-anchored protein *LYPD1* was preferentially expressed in the dental papilla (Fig. 1B). In E16 mice, real-time quantitative RT-PCR (qRT-PCR) analysis showed that *Lypd1* expression was higher in the teeth and brain than in the eyes, colon, heart, kidney, liver, lung, skin, and stomach (Fig. 1C). qRT-PCR was performed for examining *Lypd1* expression using developing molars (E12–E18, postnatal day [P] 1–P7); *Lypd1* was highly expressed at E15 and E16, which are the stages involving differentiation of dental mesenchymal cells into preodontoblasts (Fig. 1D). To examine whether *Lypd1* is expressed in the dental epithelium or mesenchyme, the E16 dental epithelium was separated from the mesenchyme and qRT-PCR was performed. The results showed that *Lypd1* was highly expressed in the mesenchymal cells (Fig. 1E).

During the odontoblast differentiation process, pannexin 3 (*Panx3*) was predominantly expressed in preodontoblasts, and it has been shown to modulate the balance of preodontoblast proliferation and differentiation (15). Alkaline phosphatase (*Alpl*), which promotes mineralization, is expressed in early hard tissue formation, and dentin sialophosphoprotein (*Dspp*)

is mainly expressed in terminally differentiated odontoblasts and is considered to play an important role in the conversion of predentin to mineralized dentin (16, 17). The expression of these genes is critical for understanding the differentiation stage of odontogenesis. We further examined the expression of the odontoblast marker genes, *Panx3*, *Alpl*, and *Dspp*, in the developing tooth, and these genes showed stepwise peaks in developing tooth germ (Fig. 1, F–H). Interestingly, the expression of *Lypd1* peaked at an earlier stage of tooth development than that of the differentiation marker genes, suggesting that *Lypd1* plays an important role in the differentiation of preodontoblasts into odontoblasts.

***Lypd1* is specifically expressed in preodontoblasts**

From E16 (bell stage) onward, dental epithelial cells further differentiate into enamel-secreting ameloblasts, while their adjacent dental mesenchymal cells develop into dentin-secreting odontoblasts (12). During this period, a wider variety of cell types emerge. Hence, we performed scRNA-seq to determine the expression patterns of the *Lypd1* gene at a single-cell level. In this study, we isolated dental cells from E16 *Krt14*-RFP mice and obtained transcriptome data from 1905 single cells. Cells were categorized into eight different clusters through graph-based principal component analysis of the transcriptomic signature. The quality control statistics for the experiments are summarized in Table S2. Cell clusters were classified into cell types on the basis of known marker genes annotated in Table S3. The representative known marker genes for classification are preodontoblasts, fibroblast growth factor 3 (*Fgf3*); mesenchymal transit amplifying cells, DNA topoisomerase II alpha (*Top2a*); dental mesenchymal stem cells (DMSCs), delta like noncanonical Notch ligand 1 (*Dlk1*); dental follicle, asporin (*Aspn*); dental pulp, matrix metalloproteinase 13 (*Mmp13*); dental epithelium, keratin 14 (*Krt14*); leukocyte, TYRO protein tyrosine kinase binding protein (*Tyrbp*); and erythrocyte, 5'-aminolevulinic synthase 2 (*Alas2*) (Figs. 2, A and D and S1). Heatmap analysis was performed on the top 15 differentially expressed genes (DEGs) among the clusters. Cell type marker genes were labeled in the generated heatmap (Fig. 2B). Furthermore, we found that *Lypd1* was highly expressed in the preodontoblast cell cluster (Fig. 2C). *Lypd1* expression was similar to *Fgf3* expression, which was at the top of the list (Fig. 2D and Table S3). At the bell stage (E16–E18), *Fgf3* expression was restricted to the cuspal regions of the dental papilla mesenchyme, including preodontoblasts and differentiating odontoblasts (18). These results indicate that *Lypd1* might show specific expression in preodontoblasts.

To further understand the dental mesenchymal cell differentiation process and their gene expression, we performed trajectory analysis of an E16 molar dataset using Monocle 3 (19). In this dataset, the dental mesenchymal subset was defined as the partition that contains preodontoblast, mesenchymal transit amplifying cells, DMSC, dental follicle, and dental pulp clusters and was used for trajectory analysis (Fig. 2E). Trajectory analysis showed that the dental

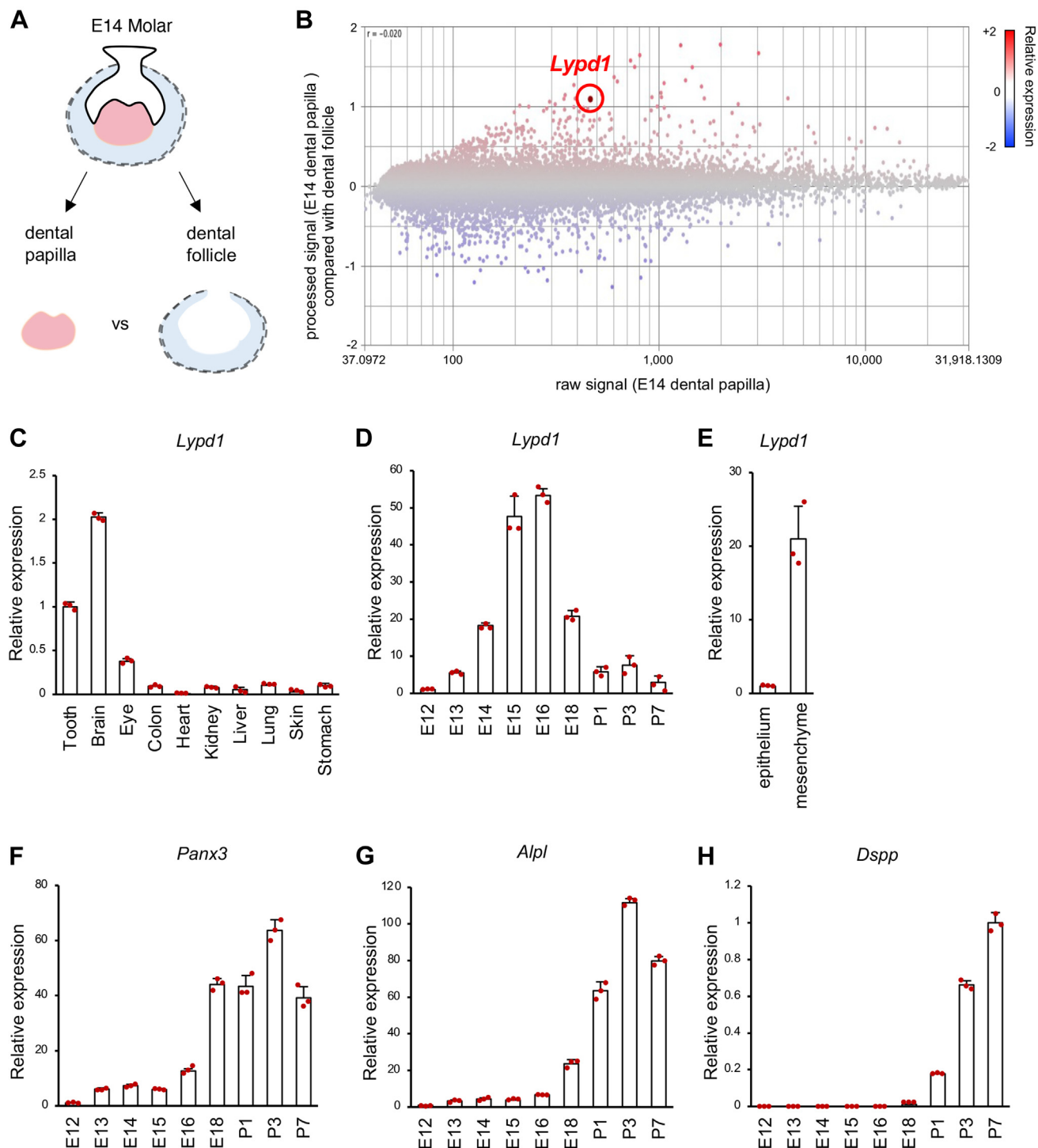


Figure 1. Expression patterns of *Lypd1* during tooth development. *A*, schematic of sample preparation of the dental papilla and dental follicle from E14 mouse molar tooth germ. *B*, gene expression profile of E14 dental papilla compared with that of the dental follicle, according to microarray analysis. The highlighted plot represents *Lypd1*. The red and blue dots indicate upregulated and downregulated genes, respectively. *C*, qRT-PCR analysis of *Lypd1* expression in the tooth, brain, eye, colon, heart, kidney, liver, lung, skin, and stomach samples from E16 embryos. *D*, qRT-PCR analysis of *Lypd1* expression in molars obtained from E12 to P7. *E*, qRT-PCR analysis of *Lypd1* expression in the dental epithelium and mesenchyme of the E16 molar. *F–H*, qRT-PCR analysis of *Panx3*, *Alpl*, and *Dspp* expression in molars obtained from E12 to P7. The mRNA expression was normalized to *Gapdh*. Error bars represent the mean \pm S.D. E, embryonic day; P, postnatal day; qRT-PCR, real-time quantitative reverse transcription polymerase chain reaction.

mesenchymal subset originated from the DMSC cluster and branched into two leaves: preodontoblast and dental follicle (Fig. 2F). As expected, *Lypd1* and *Fgf3* were highly expressed in

the preodontoblast cluster (Figs. 2G and S2B). We further used the “plot genes in pseudotime” function to examine the expression change of dental mesenchymal marker genes

LYPD1 regulates odontoblast differentiation

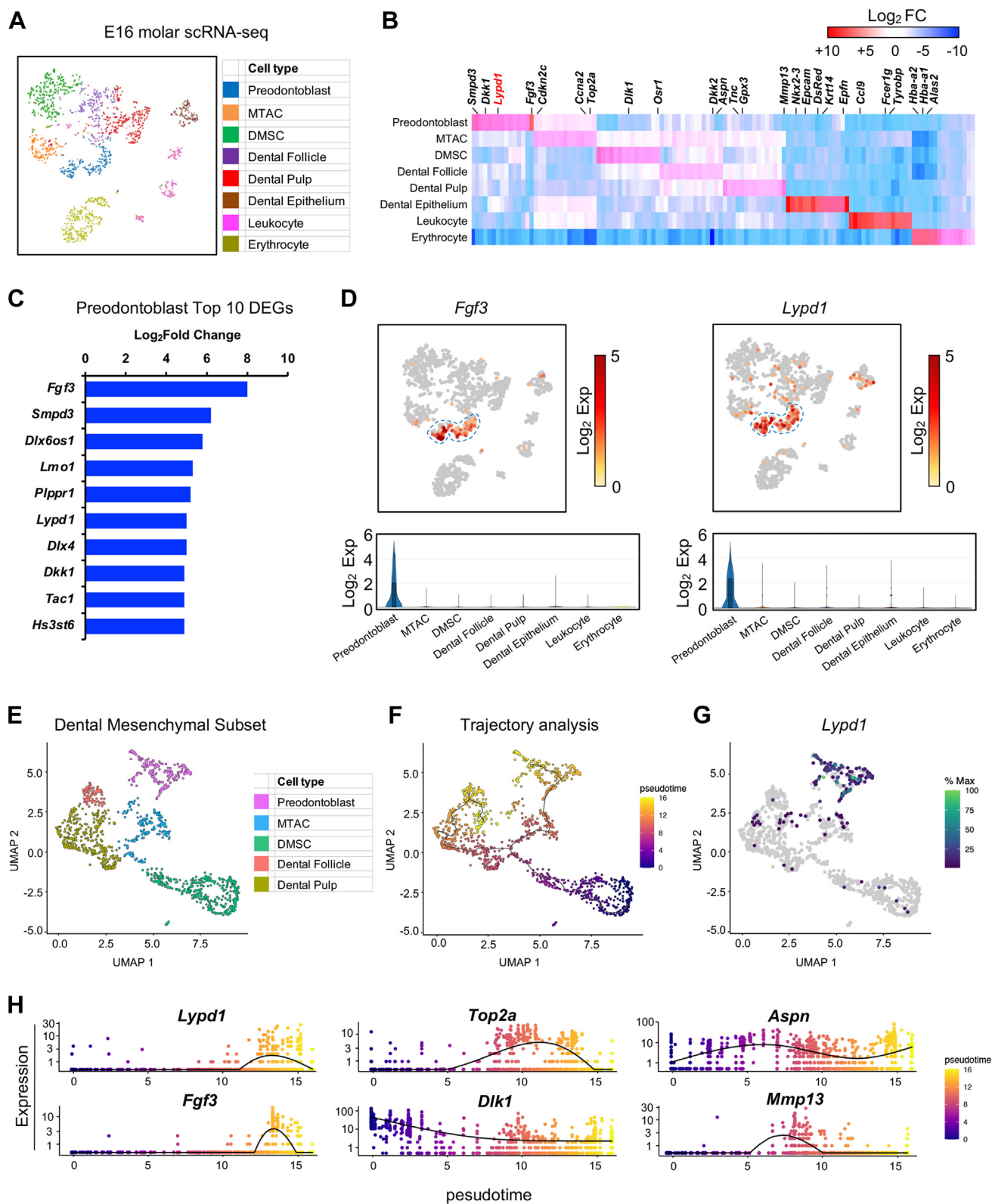


Figure 2. *Lypd1* is specifically expressed in preodontoblasts. A, t-SNE visualization of a total of 1905 single-cell datasets from E16 molars. Cells were classified by graph-based clustering. Cell types were identified using known marker genes listed in Table S3. B, heatmap analysis of the top 15 differentially expressed genes between clusters. The identity of each cluster was assigned by matching the expression profile with the expression of established cell-specific marker genes. Heatmap reports the scaled expression of discriminative gene sets for each cluster defined in (A). The labeled genes are highly expressed in each cluster. The color scheme is based on the Log_2FC from -10 (blue) to $+10$ (red). C, the top 10 differentially expressed genes (DEGs) in the preodontoblast cluster. D, expression of the preodontoblast marker *Fgf3* gene and *Lypd1* gene was projected onto the t-SNE plot (upper panel) and violin plot (lower panel). Blue dashed lines indicate the cell cluster with high gene expression. Pseudotime analyses using Monocle 3. E, dental mesenchymal subset consisting of preodontoblast, MTAC, DMSC, dental follicle, and dental pulp clusters. F, trajectory analysis of dental mesenchymal subset colored by

according to the differentiation process (Fig. 2H). The results showed that the DMSC marker *Dlk1* peaked at the early stage of differentiation, while *Lypd1* and *Fgf3* peaked at late stage of differentiation (Fig. 2H), suggesting that *Lypd1* is a novel differentiation marker of preodontoblasts.

LYPD1 is localized in lipid rafts and is essential for tooth development

To examine the localization of *Lypd1* during tooth development, we performed *in situ* hybridization (ISH) using molars at E14, E15, and E16 (Fig. 3A). The result showed that *Lypd1* was intensely expressed in the dental papilla of the developing tooth. During the cap stage (E14), *Lypd1* was broadly expressed in the condensed mesenchyme. In the early bell stage (E15), significant expression of *Lypd1* was observed in the dental papilla near the inner enamel epithelium, which are presumptive odontoblast-forming cells. Furthermore, its expression was observed in preodontoblast cells along the inner enamel epithelium at the bell stage (E16) (Fig. 3A).

The notable characteristic of GPI-APs is their association with raft membrane microdomains (20). To investigate whether LYPD1 is localized to rafts, detergent-resistant membrane (DRM) fractions from mouse dental pulp (mDP) cells treated with or without methyl- β -cyclodextrin (M β CD), a lipid-raft inhibitor, were floated on an OptiPrep step gradient. DRMs are one biochemical definition of lipid rafts since they are insoluble in nonionic detergents at 4 °C (21). Caveolin-1, a marker for DRM fractions, was detected in fractions 4, 5, and 6, indicating that these fractions contained DRMs. (Fig. 3B, left panel, below panel). We found that LYPD1 was enriched in the DRM fractions by Western blot analysis (Fig. 3B, left panel, upper panel). On the other hand, LYPD1 and Caveolin-1 were shifted to a membrane region other than the DRM domain after the destruction of lipid rafts by M β CD treatment (Fig. 3B, right panel). The results suggest that LYPD1 is localized to the lipid rafts of mDP cells.

We examined the role of *Lypd1* in tooth development using an *ex vivo* organ culture system. In this system, we can directly assess the effect of transfection of siRNA or addition of reagents on organ development. We selected *Lypd1* SMARTpool siRNA (a mixture of four distinct siRNAs targeting *Lypd1* gene) with modified chemistry to reduce off-target effects (Dharmacon RNA Technologies) for silencing the expression of *Lypd1*. We tested the ability of each of the four siRNAs to silence *Lypd1* expression and the influence on the differentiation of mDP cells. The results showed that *Lypd1* SMARTpool siRNA and all four siRNA sequences decreased *Lypd1* and *Dspp* expression compared with the negative control (Fig. S3). *Lypd1* SMARTpool siRNA was therefore used for subsequent experiments to avoid the possibility of off-target effects. E15 mandibular tooth germs were dissected, and knockdown experiments of *Lypd1* were performed using control or *Lypd1* siRNA (Fig. 3C). Upon transfection of *Lypd1*

siRNA into the tooth germs, the mRNA and protein expression levels of *Lypd1* and odontoblast differentiation marker genes (*Panx3*, *Alpl*, *Dspp*) and proteins were significantly downregulated (Fig. 3, D and E). Since odontoblast differentiation was impaired following *Lypd1* depletion in E15 tooth organ culture, histological differences in the odontoblasts were compared between the molars transfected with control and *Lypd1* siRNA. In the control molars, odontoblast cells differentiated and were highly columnar, polarized, and neatly arranged. By contrast, *Lypd1* siRNA-transfected molars had layers of nonpolarized cuboidal cells with a centrally located nucleus and were randomly arranged (Fig. 3, F and G), suggesting that the differentiation of odontoblasts is disturbed by depletion of *Lypd1*. In addition, immunohistochemistry of molars revealed that the expression of ALPL was suppressed in the odontoblasts of *Lypd1*-depleted molars (Fig. 3F). These results suggest that *Lypd1* plays an important role in the differentiation of dental mesenchymal cells.

Lipid rafts are essential for cell differentiation in the developing tooth

Next, we analyzed the effect of lipid rafts on tooth development using the *ex vivo* organ culture system. E15 mandibular tooth germs were dissected and treated with lipid raft-targeting drugs, including M β CD, simvastatin, and fumonisin B1 (Fig. 4A). We found that the mRNA and protein expression levels of LYPD1 and odontoblast differentiation marker genes were significantly downregulated in the lipid raft-targeting drug-treated tooth germs (Fig. 4, B–D). We confirmed that the other two lipid raft-targeting drugs, zaragozic acid A and myriocin, also downregulated LYPD1 and odontoblast differentiation marker genes (Fig. S4, A and B). Similar results were obtained in the M β CD-treated mDP cells (Fig. S5). These results suggest that LYPD1 and lipid raft formation are essential for cell differentiation in the developing tooth.

LYPD1 is necessary for the differentiation of dental mesenchymal cells, and it induces odontoblast differentiation via the bone morphogenetic protein signaling pathway

Because various signaling pathways are involved in odontoblast differentiation (22, 23), we examined the phosphorylation of signal cascade molecules to determine the signaling pathways triggered by LYPD1. mDP cells were transfected with control or *Lypd1* siRNA, and then the phosphorylation of signaling molecules was evaluated by Western blotting. We observed a significant decrease in Smad1/5/8 phosphorylation in mDP cells transfected with *Lypd1* siRNA after 48 h of culture. However, the phosphorylation of Smad2 or Smad3 was not detected. No significant change was observed in Akt phosphorylation and β -catenin phosphorylation (Fig. 5A, left panel). The results suggested that LYPD1 is involved in the phosphorylation of Smad1/5/8. Similarly, we examined

pseudotime. G, expression of *Lypd1* is projected onto the UMAP plot. H, the results of "plot genes in pseudotime" function in dental mesenchymal subset. Graph shows the expression change of dental mesenchymal marker genes according to pseudotime. DMSC, dental mesenchymal stem cell; MTAC, mesenchymal transit amplifying cell; t-SNE, t-distributed stochastic neighbor embedding; UMAP, Uniform Manifold Approximation and Projection.

LYPD1 regulates odontoblast differentiation

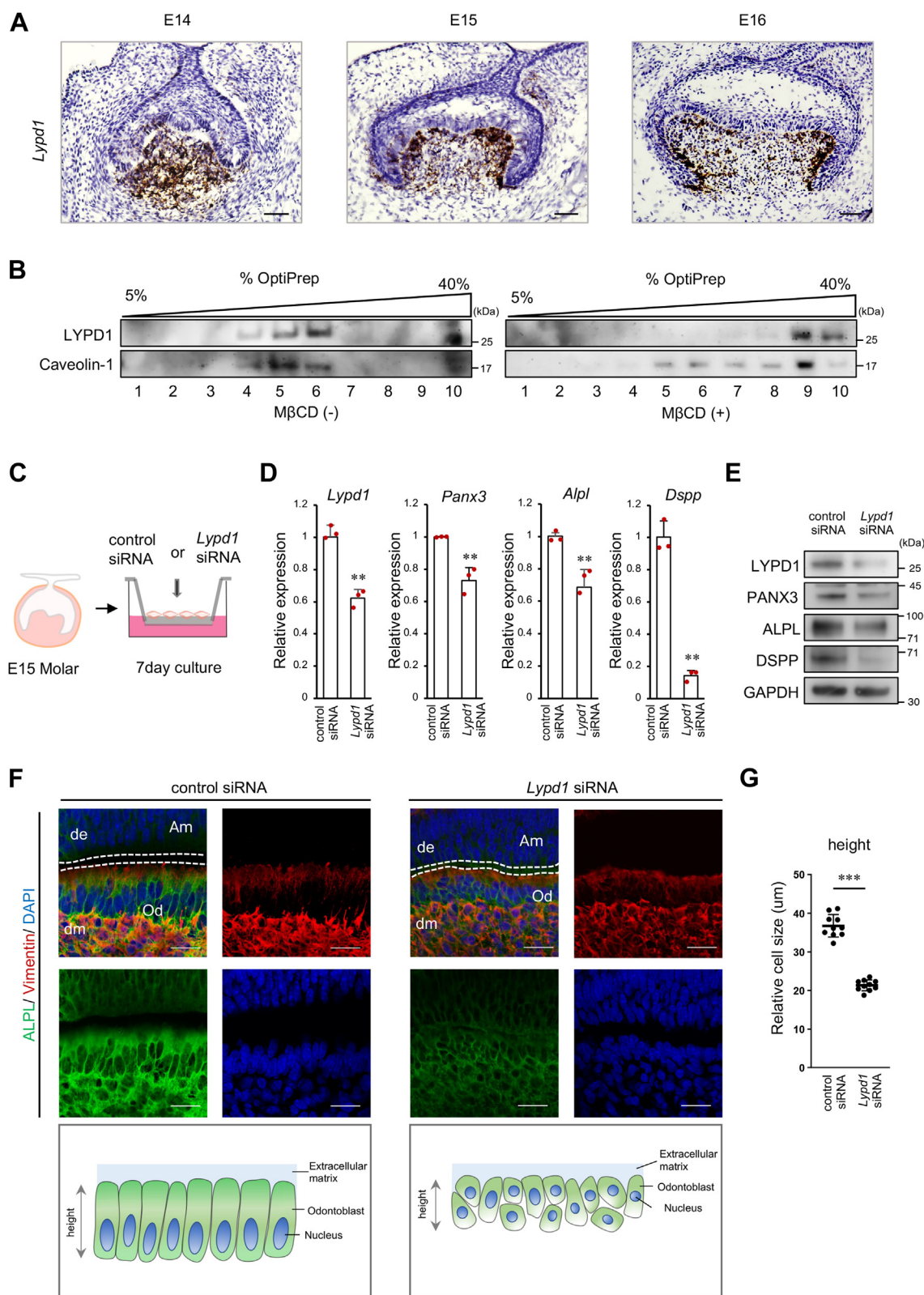


Figure 3. LYPD1 localized in lipid rafts and was essential for tooth development. *A*, *in situ* hybridization of *Lypd1* in developing molars. Expression of *Lypd1* mRNA was detected using the probe of *Lypd1* in E14, E15, and E16 mouse molar semiserical sections. *Brown*, *Lypd1*; *purple*, nucleus. The scale bars represent 50 μm . *B*, fractionation of mDP cells treated with or without M β CD (1 mM) into soluble and detergent-resistant membranes. The localization of endogenous LYPD1 and Caveolin-1 was detected by Western blot. Caveolin-1 was used as a marker to identify detergent-resistant membrane fractions. *C*, general schematic representation of the experimental procedure used for organ culture. *D*, real-time quantitative RT-PCR analysis of *Lypd1*, *Panx3*, *Alpl*, and *Dspp* expression in E15 tooth germs transfected with control or *Lypd1* siRNA after 7 days of culture. The mRNA expression was normalized to *Gapdh*. *E*, Western blotting results for LYPD1, PANX3, ALPL, DSPP, and GAPDH in E15 tooth germs transfected with control or *Lypd1* siRNA after 7 days of culture. GAPDH was used as the internal control. *F*, *upper panel*, immunofluorescence of ALPL (*green*) and vimentin (*red*) in the section of E15 tooth germs cultured

whether these signaling pathways were affected by treatment of mDP cells with M β CD and whether this resulted in the disruption of lipid rafts. By contrast to observations under *Lygd1* inhibition, we detected a reduction not only in Smad1/5/8 phosphorylation in the M β CD-treated group but also in Akt phosphorylation and β -catenin phosphorylation (Fig. 5A, right panel). These results confirm that lipid rafts are a platform for signaling pathways and that various signaling pathways may be affected when the lipid raft structure is disrupted. The bone morphogenetic protein (BMP)/Smad signaling pathway plays a significant role in odontoblast differentiation (24). To confirm the involvement of LYPD1 in BMP signaling pathway, we examined the level of BMP2-mediated Smad1/5/8 phosphorylation in control and *Lygd1*-depleted mDP cells. In *Lygd1*-depleted mDP cells, BMP2-mediated phosphorylation of Smad1/5/8 was downregulated (Fig. 5B). Since Id1 is a direct target of the BMP/Smad signaling pathway (25), we investigated whether the expression of Id1 is affected by knockdown of *Lygd1* expression in mDP cells. We found that, when *Lygd1* was depleted, Id1 expression decreased along with reduced level of phosphorylation of Smad1/5/8 protein (Fig. 5B). These results suggest that LYPD1 induces odontoblast differentiation by participating in the BMP/Smad signaling pathway.

BMP2 is an important regulator of odontoblast differentiation, and BMP2 treatment promotes differentiation of mDP cells into *Dspp*-expressing odontoblasts (15, 26). We further analyzed the molecular mechanism of LYPD1-mediated dental mesenchymal cell differentiation by transfecting mDP cells with control or *Lygd1* siRNA and subsequently culturing them in the presence or absence of BMP2 (Fig. 5C). The marker genes are expressed sequentially during odontoblast differentiation in the following order: *Lygd1*, *Panx3*, *Alpl*, and *Dspp* (Fig. 1, D, F, G, and H). We reproduced this odontoblast differentiation process in mDP cells and found that BMP2 induces the expression of *Alpl* and *Dspp* (Fig. 5C). *Lygd1* knockdown in mDP cells inhibited *Panx3*, *Alpl*, and *Dspp* expression (Fig. 5, C and D). To further investigate the effect of LYPD1 on mDP cell differentiation, we performed an ALP assay and ALP staining. mDP cells transfected with *Lygd1* siRNA showed a lower ALP activity than the control cells (Fig. 5E). Similarly, the results of ALP staining showed that inhibition of *Lygd1* resulted in a decrease in ALPL expression (Fig. 5F). These findings suggest that LYPD1 plays an important role in dental mesenchymal cell differentiation and that it is required for odontoblast differentiation.

The GPI structural domain of LYPD1 is essential for odontoblast differentiation

GPI-APs are posttranslationally modified by glycolipids known as GPI anchors, which allow them to attach and localize to the plasma membrane (10). According to

bioinformatics analyses, the mouse LYPD1 protein sequence has been predicted to comprise a potential signal peptide sequence, as well as a potential C-terminal GPI anchor attachment site, known as the omega site (Fig. 6A). For a better understanding of the function of LYPD1 as a GPI-AP, we generated constructs of LYPD1, including full-length LYPD1 (LYPD1-FL) and a truncated construct lacking the C-terminal domain containing the omega site (LYPD1- Δ GPI) (Fig. 6B). Interestingly, the LYPD1-FL-GFP-positive cells showed morphological changes, such as a columnar and polarized morphology with long dendrite-like protrusions compared with mock-GFP-transfected cells (Fig. 6C). However, the LYPD1- Δ GPI-GFP-positive cells showed no difference compared with the mock-GFP-transfected cells. LYPD1-FL-GFP-positive cells were characterized by longer cell length, smaller cell area, and fewer cell protrusions. Nevertheless, most LYPD1- Δ GPI-GFP-positive cells were morphologically similar to the control cells, maintaining a fibroblast-like morphological appearance with a stellate or polygonal shape (Fig. 6, C and D). We subsequently created constructs of V5-His tagged LYPD1-FL and LYPD1- Δ GPI and analyzed the expression of *Panx3* and *Dspp* (Fig. 6E). The LYPD1-FL-transfected group exhibited significantly upregulated *Panx3* and *Dspp* expressions compared with the LYPD1- Δ GPI-transfected group (Fig. 6E).

To further assess the importance of the omega site of LYPD1 for cell differentiation, we performed flow cytometry using LYPD1-FL-GFP- and LYPD1- Δ GPI-GFP-transfected mDP cells (Fig. 6F). To sort the GFP-positive cells, hierarchical gates of mDP cells not transfected on the FSC-A/SSC-A subset, the FSC-H/FSC-W subset, and the SSC-H/SSC-W subset were set. Using a cell sorter, we isolated negative control cells and GFP-positive cells separately and performed qRT-PCR (Fig. 6G). The expression of *Panx3* was significantly upregulated in the LYPD1-FL-GFP cell population compared with that in the LYPD1- Δ GPI-GFP cell population (Fig. 6G), consistent with the results in Figure 6E. For further analysis of the mechanisms, mDP cells were transfected with the mock, LYPD1-FL, and LYPD1- Δ GPI expression vectors, and the phosphorylation of Smad1/5/8 was evaluated by Western blotting. Smad1/5/8 phosphorylation increased from 5 to 30 min after addition of recombinant BMP2 in mDP cells transfected with LYPD1-FL rather than the LYPD1- Δ GPI expression vector (Fig. S6). These findings suggest that LYPD1 plays a crucial role in the differentiation of mDP cells through binding to the GPI anchor, implying that the plasma membrane localization of LYPD1 is important.

Discussion

In this study, we identified that LYPD1 is highly expressed at a specific stage of preodontoblast differentiation and acts as a

for 7 days after transfection with control siRNA or *Lygd1* siRNA. Nuclei were stained with DAPI (blue). Vimentin was used as a marker of the dental mesenchyme. White lines represent the basement membrane of teeth. Lower panel, diagram of odontoblast cells in E15 tooth germs transfected with control siRNA or *Lygd1* siRNA. de, dental epithelium; dm, dental mesenchyme; Am, Ameloblasts; Od, odontoblasts. The scale bars represent 20 μ m. G, the height of odontoblast cells in E15 molar transfected with control siRNA or *Lygd1* siRNA and cultured for 7 days. Quantification was performed using the ImageJ software. ** p < 0.01; *** p < 0.001. Error bars represent the mean \pm SD. E, embryonic day.

LYPD1 regulates odontoblast differentiation

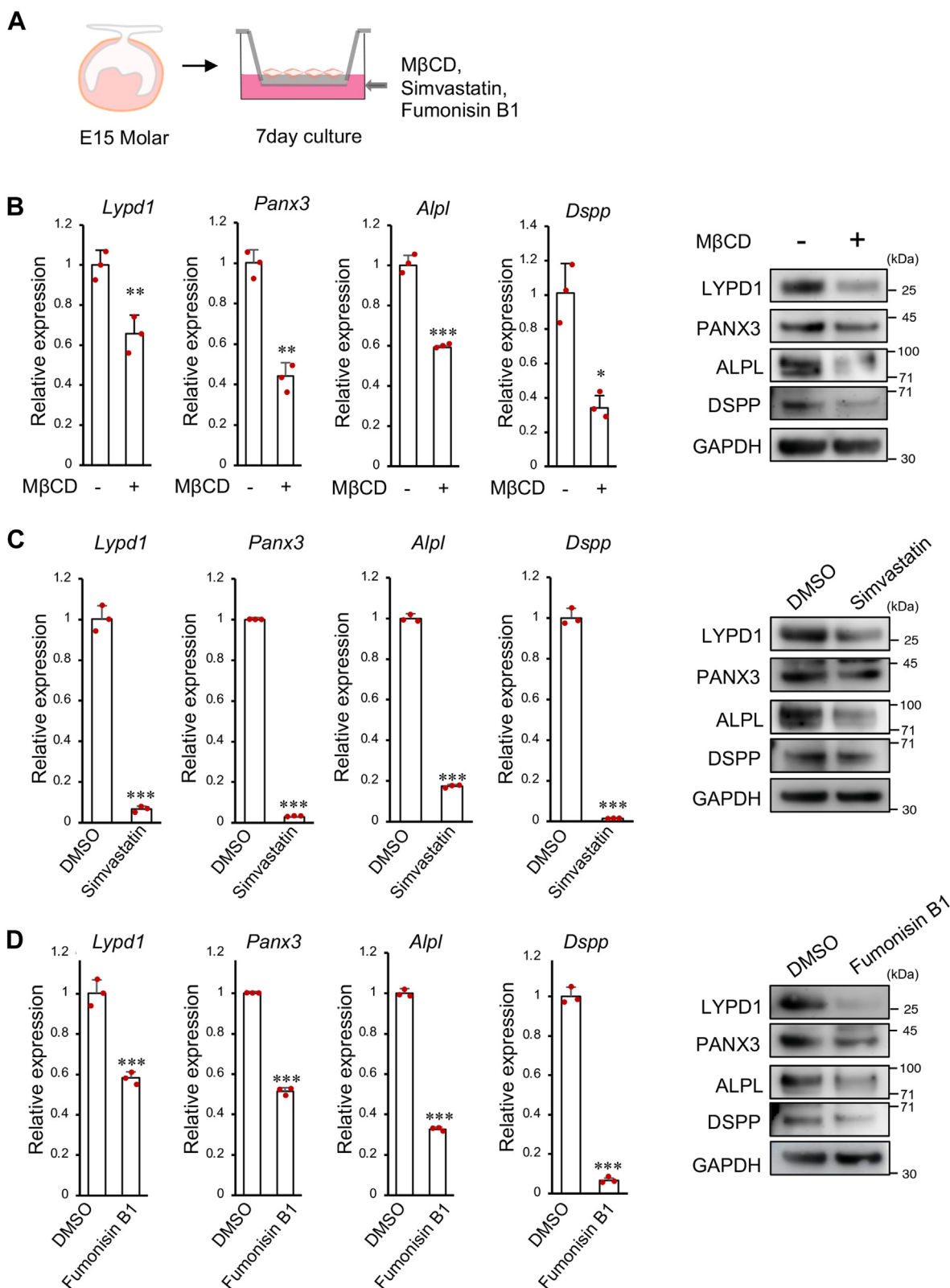


Figure 4. Lipid rafts are essential for cell differentiation in the developing tooth. A, general schematic representation of the experimental procedure used for organ culture. B–D, left, real-time quantitative RT-PCR analysis of E15 tooth germs treated with DMSO or 1 mM MβCD, 1 μM Simvastatin, 40 μM Fumonisin B1 cultured for 7 days. The expressions of *Lypd1*, *Panx3*, *Alpl*, and *Dspp* were normalized to *Gapdh* mRNA expression. * $p < 0.05$; ** $p < 0.01$; *** $p < 0.001$. Error bars represent the mean \pm SD. B–D, right, Western blotting results of LYPD1, PANX3, ALPL, DSPP, and GAPDH in E15 tooth germs treated with DMSO or 1 mM MβCD, 1 μM Simvastatin, or 40 μM Fumonisin B1 cultured for 7 days. GAPDH was used as the internal control. DMSO, dimethyl sulfoxide.

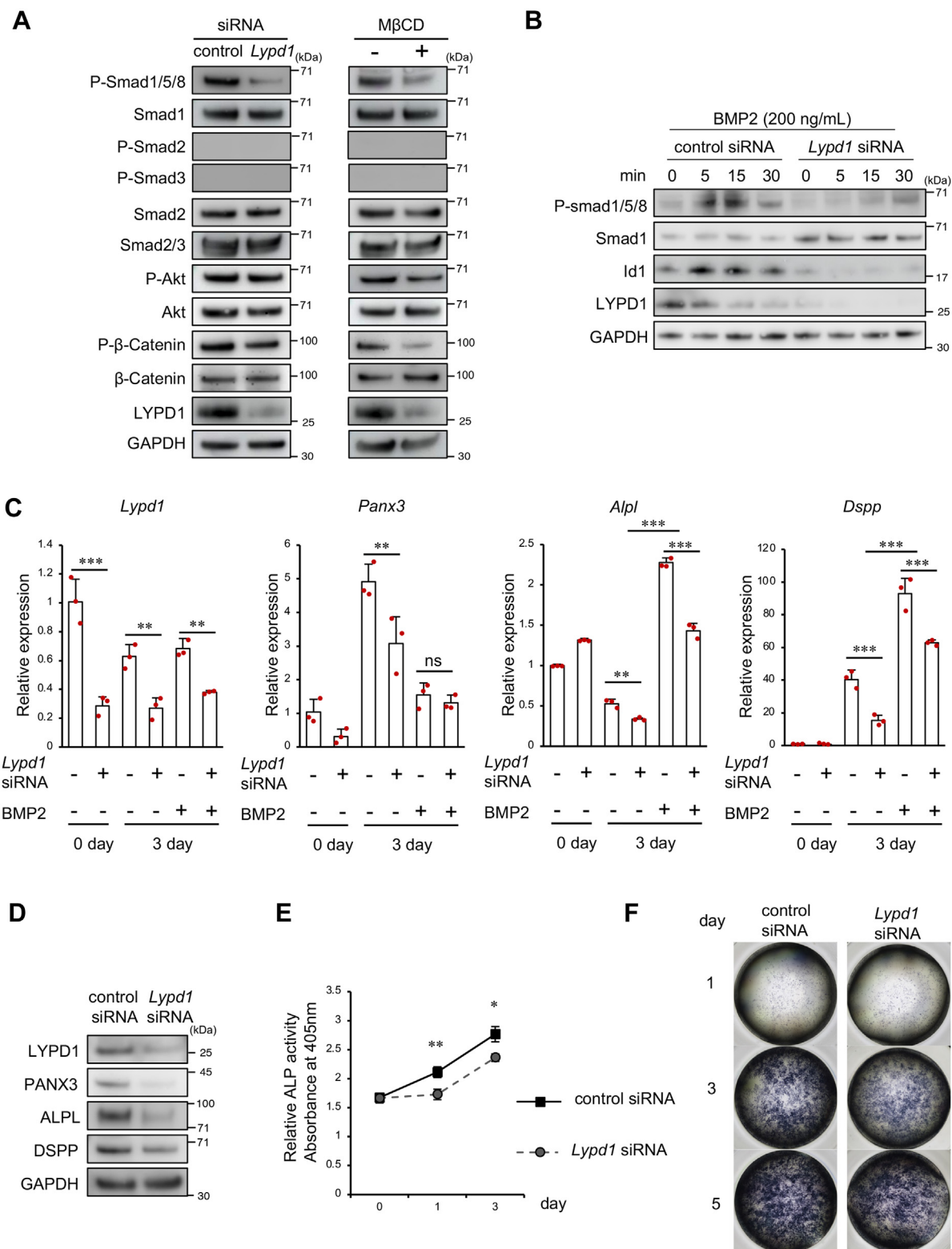


Figure 5. LYPD1 regulates odontoblast differentiation via BMP-Smad1/5/8 signaling pathway. *A*, Western blotting of P-Smad1/5/8, Smad1, P-Smad2, P-Smad3, Smad2, Smad2/3, P-Akt, Akt, P- β -Catenin, β -Catenin, LYPD1, and GAPDH in mDP cells transfected with control siRNA and *Lypd1* siRNA (left panel) or treated with M β CD (0 mM, 1 mM) (right panel) and cultured for 48 h. GAPDH was used as the internal control. *B*, Western blotting results of BMP2-induced Smad1/5/8 phosphorylation in mDP cells transfected with control siRNA or *Lypd1* siRNA. After 48 h of transfection with control siRNA and *Lypd1* siRNA, mDP cells were stimulated with 200 ng/ml BMP2 for 0, 5, 15, and 30 min. Protein extractions were analyzed by Western blotting using anti-phospho-Smad1/5/8, anti-Smad1, anti-Id1, anti-LYPD1, and anti-GAPDH antibodies. GAPDH was used as the internal control. *C*, real-time quantitative RT-PCR analysis of *Lypd1*, *Panx3*, *Alpl*, and *Dspp* expression in mDP cells transfected with either control siRNA or *Lypd1* siRNA, cultured with or without 200 ng/ml BMP2 for 3 days after transfection. The mRNA expression was normalized to *Gapdh*. ns, $p > 0.05$; ** $p < 0.01$; *** $p < 0.001$. Error bars represent the mean \pm SD. *D*, Western blotting results of LYPD1, PANX3, ALPL, DSPP, and GAPDH in mDP cells transfected with either control siRNA or *Lypd1* siRNA. GAPDH was used as the internal control. *E*, ALP activity of mDP cells after transfection with control or *Lypd1* siRNA. * $p < 0.05$; ** $p < 0.01$ compared with the value in the control siRNA group.

LYPD1 regulates odontoblast differentiation

GPI-AP in lipid rafts. In lipid rafts, LYPD1 regulated odontoblast differentiation by associating with BMPR and induced phosphorylation of Smad1/5/8 (Fig. 7).

GPI-APs associated with lipid raft microdomains have been reported to regulate various signaling pathways, such as TGF- β , GDNF/Ret, BMP, and Wnt signaling, by rearranging receptor complexes in the plasma membrane (27–30). Lymphocyte antigen-6 (Ly6) family members have been reported to exhibit a common function of modulating receptor-mediated signaling (31, 32). LYPD1 belongs to the Ly6/urokinase-type plasminogen activator receptor superfamily, which is classified into two subfamilies according to their subcellular localization. One comprises proteins attached to the cell surface by a GPI anchor, and the other comprises secreted proteins (33). Lipid raft components, including GPI-AP, can be isolated in DRM fraction because of the resistance of lipid rafts to certain nonionic detergents, such as Triton X-100 (21). Although there is consensus that DRMs do not reflect lipid rafts on cell membranes (34), the presence of molecules in the DRM fractions of cell extracts can be interpreted as a sign that they are preferred to partition into rafts in living cells (35). In this study, by subcellular fractionation using an OptiPrep density gradient, LYPD1 was isolated in DRMs. Nevertheless, when the lipid rafts were disrupted by treatment with M β CD, LYPD1 was shifted to the detergent-soluble fractions. This result indicates the possibility of LYPD1 localization in lipid rafts of mDP cells. In this study, we identified that the C terminus containing the omega site of LYPD1 is critical for cell differentiation, suggesting that LYPD1 plays a role as a GPI-AP in odontoblast differentiation. GPI-anchored Ly6/urokinase-type plasminogen activator receptor proteins accumulate at lipid rafts on the cell surface and interact with signaling molecules to modulate signaling (33). In mice, this superfamily contains eight LYPD family molecules, including *Lypd2*, *Lypd4*, and *Lypd8*, which are reported to exhibit organ-specific expression (36, 37). We analyzed the expression of LYPD family using scRNA-seq and found no factors other than *Lypd1* that were expressed specifically in the tooth (Fig. S7). Although LYPD1 is a GPI-AP, few studies have been reported regarding its role in organ development.

Herein, we confirmed the effect of lipid rafts on tooth development using an *ex vivo* organ culture system with five different lipid raft-targeting drugs. Among them, M β CD binds strongly to cholesterol, is known to disrupt lipid raft structures, and is the most used cholesterol remover when analyzing lipid rafts (38). Simvastatin is an inhibitor of the rate-limiting enzyme HMG-CoA in the cholesterol biosynthesis pathway and not only reduces the cholesterol present on the plasma membrane but also inhibits cholesterol synthesis *via* the intracellular cholesterol biosynthesis pathway (39). Fumonisin B1 is a ceramide synthase inhibitor and blocks the biosynthesis of sphingolipids, which are a critical component of lipid rafts (40). Zaragozic acid A is an inhibitor of squalene synthase in the cholesterol biosynthesis pathway (41), and

myriocin is an inhibitor of serine palmitoyl transferase and affects sphingolipid biosynthesis (42). According to these results, all lipid raft-targeting drug-treated tooth germs showed a decrease in the expression of LYPD1 and odontoblast differentiation markers at both the RNA and protein levels. Tooth development was hindered by either destroying lipid rafts by removing cholesterol from them or inhibiting the synthesis of cholesterol and sphingolipids (which are essential components of lipid rafts). Therefore, we suggest that lipid rafts may play an important role in tooth development.

Previously, we used bioinformatics tools, such as microarray analysis, cap analysis of gene expression, or scRNA-seq, to identify some molecules important for tooth development (43–47). Transcriptome analysis, including scRNA-seq, is commonly used for screening gene expression, and various datasets obtained from the tooth germ have been deposited in a repository (48–50). Although these studies identified many candidates as novel marker genes for various dental cell types, the roles of these marker genes have not been elucidated yet. Krivanek *et al.* (50) reported that *Foxd1* and *Fgf3* are colocalized in the incisor dental pulp, which contains a stem cell niche for dental mesenchymal lineage, near the inner enamel epithelium. Surprisingly, *Lypd1* was highly expressed in the cluster of *Foxd1+* cells in their scRNA-seq datasets. In this study, microarray analysis indicated that the dental papilla specifically expressed *Lypd1*. scRNA-seq analysis revealed that *Lypd1* was specifically expressed in the preodontoblast clusters; this result was validated by ISH. These results prove that *Lypd1* is a novel preodontoblast marker and a functionally essential gene for odontoblast differentiation. Furthermore, we report the scRNA-seq atlas of E16 molar. This gene expression profile would contribute to further characterization of the early stages of the dental cell development process, especially the gene expression signature of preodontoblasts.

During tooth morphogenesis, various signaling pathways, such as BMP, Wnt, Notch, Fgf, and Shh, are activated (12). BMP2 is one of the most significant growth factors that mediate tooth development, particularly the differentiation of odontoblasts (51, 52). BMP2 is expressed actively at the cap stage and bell stage, and dentin sialophosphoprotein (DSPP) is expressed at the secretory stage (24). BMP2 signaling is delivered into cells *via* a heterotetrameric complex of serine/threonine kinase-active type II and type I receptors. Smads are phosphorylated and activated when BMP2 binds to BMPR (53). Consistent with this result, we found that BMP2 induced the expression of *Alpl*, and *Dspp* in mDP cells, while their expression was reduced when *Lypd1* was inhibited. In this study, we determined that LYPD1 is involved in the phosphorylation of Smad1/5/8 by examining the phosphorylation of signal cascade molecules, whereas lipid raft inhibition also reduced the other signaling pathway. This also confirmed the function of lipid rafts as a platform for signal transduction. These results suggest that LYPD1 specifically regulates the BMP2-Smad1/5/8 signaling pathway and may help induce

Error bars represent the mean \pm SD. F, ALP staining of mDP cells on days 1, 3, and 5 after transfection with control siRNA (left panel) and *Lypd1* siRNA (right panel). ALP, alkaline phosphatase; ns, nonsignificant.

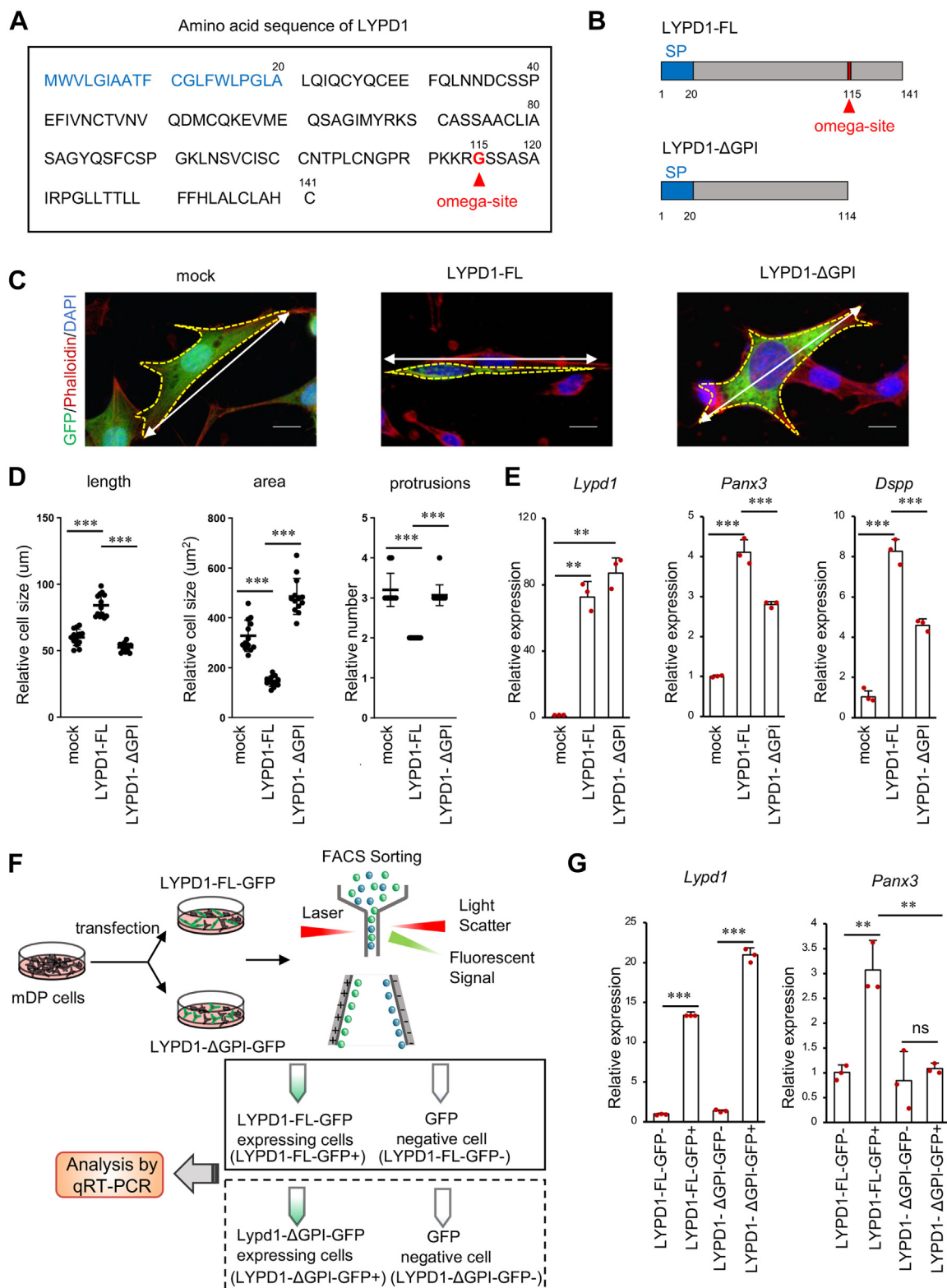


Figure 6. LYPD1 promotes odontoblast differentiation via the GPI structural domain. *A*, amino acid sequence of LYPD1. The N-terminal amino acids 1–20 were signal peptide (letters are shown in blue). GPI-anchor attachment site (omega site) was predicted at position 115:G (the letter indicated by the red triangle) using big-PI Predictor (I.M.P. Bioinformatics). The C-terminal amino acids 115 to 141 were deleted in the truncated construct. *B*, domain structure of wildtype (LYPD1-FL) and C-terminally truncated LYPD1 (LYPD1-ΔGPI). LYPD1-FL, full-length LYPD1; LYPD1-ΔGPI, with deletion of the C-terminal 115 to 141. SP, signal peptide (blue section). *C*, mDP cells were transfected with mock-GFP (left panel), LYPD1-FL-GFP (middle panel), or LYPD1-ΔGPI-GFP (right panel) and cultured for 48 h. Expression of GFP (green) and phalloidin (red) was detected by immunocytochemistry and visualized using a Zeiss LSM700 confocal laser scanning microscope. Nuclei were stained with DAPI (blue). The white arrow solid line and yellow dotted line were used for measuring the length and area of mDP cells, respectively. The scale bars represent 20 μm. *D*, the length, area, and cellular protrusions of mDP cells transfected with mock-GFP, LYPD1-FL-GFP, or LYPD1-ΔGPI-GFP. Quantification was performed using the ImageJ software. ****p* < 0.001. Error bars represent the mean ± SD. *E*, real-time quantitative RT-PCR analysis of *Lypd1*, *Panx3*, and *Dspp* expression levels in mDP cells transfected with mock, LYPD1-FL, or LYPD1-ΔGPI and cultured for 48 h. ***p* < 0.01;

LYPD1 regulates odontoblast differentiation

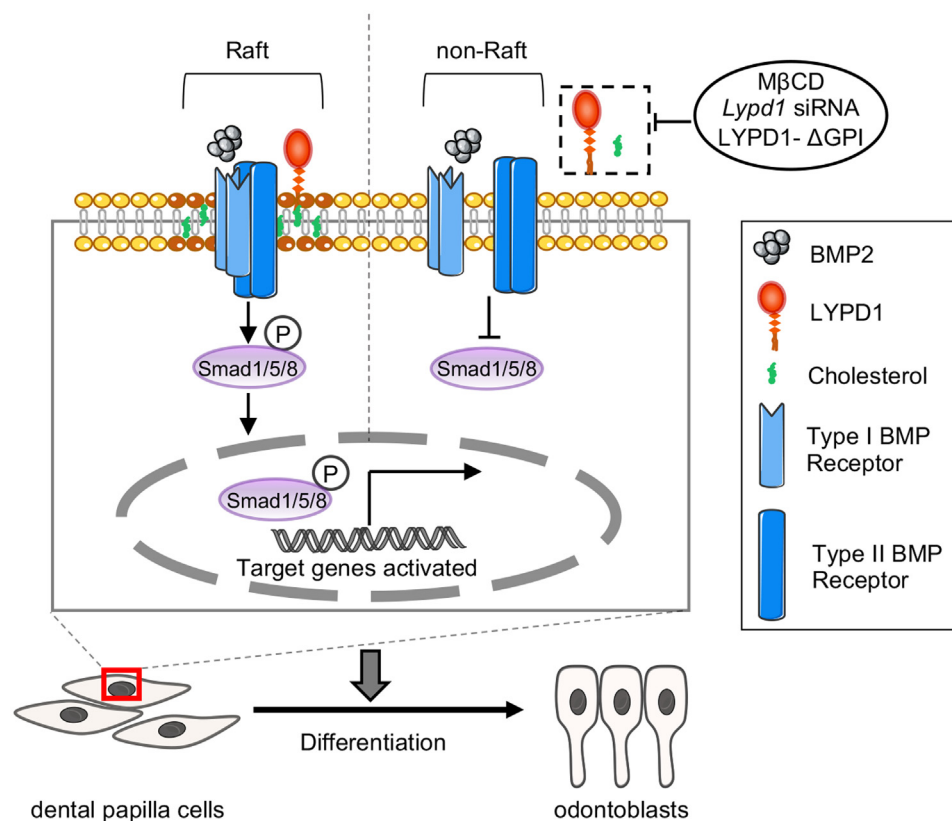


Figure 7. Summary diagram of the effect of LYPD1 as a GPI-anchored protein during tooth development. Model of LYPD1 function as a GPI-anchored protein in the differentiation of dental papilla cells to odontoblasts.

odontoblast differentiation. However, it is unclear how *Lypd1* is regulated during tooth development, and thus identifying factors that regulate *Lypd1* is our next challenge.

Morphological change is a unique characteristic of DPCs during odontoblast differentiation. Once DPCs differentiate into odontoblasts, they change their morphology; for example, the polygonal cells become columnar and polarized, with long dendritic processes (54). In this study, the morphological change of odontoblasts was observed by inhibiting *Lypd1* in *ex vivo* organ culture system. To confirm this, we created LYPD1-FL and LYPD1-ΔGPI constructs to analyze the function of LYPD1 as a GPI-AP. We found that cells over-expressing LYPD1 showed morphological features similar to those of odontoblasts, such as a columnar and polarized morphology with long protrusions. In contrast, the morphology of the cells transfected with the deletion construct of the omega site did not change significantly compared with the control, showing a fibroblast-like cell morphology with a polygonal shape. Furthermore, we found that not LYPD1-ΔGPI but LYPD1-FL promotes the differentiation of mDP cells. These results suggest that LYPD1 as a GPI-AP mediates odontoblast-like morphological changes and differentiation.

In summary, LYPD1 is specifically expressed in pre-odontoblasts, and it plays a crucial role as a lipid raft

component in BMP-mediated odontoblast differentiation. These findings uncover novel mechanisms in the dental papilla differentiation process and suggest the importance of lipid rafts during tooth development.

Experimental procedures

Animals

All animal experiments were performed in accordance with Animal Research: Reporting of *In Vivo* Experiments (ARRIVE) guidelines and were approved by the ethics committee of Kyushu University Animal Experiment Center (protocol no. A20-281-1), and all procedures were performed in accordance with the relevant guidelines and regulations. For sampling, pregnant mice were euthanized by medetomidine, midazolam, and butorphanol intraperitoneal administration. The embryos were dissected immediately.

Microarray analysis

Total RNA was extracted from the dental papilla and dental follicle of the lower first molar of E14 ICR mice using TRIzol reagent (Life Technologies) and purified using the RNeasy Mini kit (Qiagen) according to the manufacturer's protocol. The Experion automated electrophoresis system (Bio-Rad) was

*** $p < 0.001$. Error bars represent the mean \pm SD. F, schematic representation of cell-sorting procedures. G, real-time quantitative RT-PCR analysis of *Lypd1* and *Panx3* expression levels in LYPD1-FL-GFP- or LYPD1-ΔGPI-GFP-positive cells sorted from mDP cell suspensions using flow cytometry. ns, $p > 0.05$; ** $p < 0.01$; *** $p < 0.001$. Error bars represent the mean \pm SD. GPI, glycosylphosphatidylinositol.

used for examining the RNA quality; RNA quality indicator values for dental papilla RNA and dental follicle RNA were 10.0 and 8.4, respectively. Labeling and array hybridization were performed using standard protocols at the Research Support Center of the Research Center for Human Disease Modeling of Kyushu University. Gene expression profiles were analyzed using a chip-based gene array (MouseWG-6 version 2, Illumina) and normalized in Genome Studio (Illumina). Gene expression analyses were performed using Subio Platform 1.18 (Subio).

scRNA-seq analysis

Tissue sample dissociation, single-cell library preparation, and single-cell RNA-seq data analysis were performed as described (55). The first molars of the lower mandible were collected from the littermates of E16 Krt14-RFP mice. Dissected molars were enzymatically processed with Accutase (Sigma-Aldrich) for 30 min at 37 °C. Thereafter, the cells obtained were resuspended in cold phosphate-buffered saline (PBS) containing 0.04% bovine serum albumin (Sigma-Aldrich). Single cells were isolated and a single-cell library was generated using the Chromium Single Cell 3' Reagent Kit (10x Genomics) according to the manufacturer's protocol. As described (55), the libraries were sequenced on a NextSeq 500 sequencer (Illumina). From the molars of E16 Krt14-RFP mice, a total of 1905 cells were identified for subsequent clustering evaluation. Data processing was performed using the 10x Genomics Workflow (56). The Cell Ranger Single Cell Software Suite v2.1.0 (10x Genomics) was used for demultiplexing, barcode assignment, and unique molecular identifier quantification. Cells for which <200 genes were detected were excluded from subsequent analysis. Cells with >10% unique molecular identifiers mapped to mitochondrial genes were defined as nonviable or apoptotic cells and were not included in the analyses. Clustering and gene expression were visualized using a Loupe Cell Browser v6 (10x Genomics). For visualizing data in 2D space, the PCA-reduced data were projected onto the t-Stochastic Neighbor Embedding plot. Clusters were defined by the graph-based clustering algorithm. The *p*-values were adjusted using the Benjamini–Hochberg correction for multiple tests. Under the following conditions, we considered genes to be differentially expressed: log₂-fold change of >1.0 and *p*-value <0.1. Thereafter, clusters were labeled on the basis of known dental cell marker genes observed in the top 20 upregulated DEGs between clusters. Heatmap analysis was performed using the Loupe Cell Browser for the top 15 upregulated DEGs of the preodontoblast cluster.

For trajectory analysis, Monocle 3 software (19) was used under R version 4.2.2. A total of 1905 cell datasets were used as input, and the clustering was performed with a resolution of 0.003. For visualizing data in 2D space, the dataset was pre-processed with PCA in dimension = 50, and uniform manifold approximation and projection was used for reduction. The command “learn_graph” was implemented in default setting, and the root node was manually selected from the edge of the DMSC cluster with the “order_cells” function.

In situ hybridization

ICR mouse heads (E14, E15, and E16) were fixed with 4% paraformaldehyde in PBS for 8 h at 4 °C and then immersed in gradient sucrose solutions in PBS for 12 to 24 h before being inserted into the optimal cutting temperature compound (Sakura Finetek). Sections (10 μm thick) were cut, and ISH was performed using RNAscope 2.5 HD Assay-BROWN (ACD, Cosmo Bio Co) according to the manufacturer's guidelines. After dehydration, the slides were treated with hydrogen peroxide at 23 °C for 10 min for removing the endogenous peroxidase contained in the tissues and incubated for 5 min at 102 °C with the target retrieval solution. After 30 min of RNAscope Protease Plus treatment at 40 °C, the *Lypd1* probe was hybridized for 2 h at 40 °C. Following hybridization, the slides were subjected to signal amplification, and hybridization signals were detected using a cocktail of diaminobenzidine solutions A and B (1:1). Finally, the slides were counterstained with Carrazi's hematoxylin (Muto Pure Chemicals Co), visualized, and photographed with a KEYENCE BZ-X800.

Cell culture and transfection

mDP cells were cultured in Dulbecco's modified Eagle's medium/F-12, supplemented with 10% fetal bovine serum (Gibco/Life Technologies) and 1% penicillin/streptomycin (Gibco/Life Technologies) at 37 °C in a 5% CO₂ humidified atmosphere. For depletion experiments of lipid rafts, mDP cells were treated with MβCD (0 mM, 1 mM, Sigma-Aldrich) for 48 h. LYPD1 expression vector or siRNA against *Lypd1* was transfected into mDP cells using a Neon Transfection System (Invitrogen) according to the manufacturer's protocol. For gene silencing, *Lypd1* SMARTpool siRNA was used (Dharmacon RNA Technologies). The SMARTpool is a mixture of four distinct siRNAs targeting the same gene. Targeted sequences of *Lypd1* used for RNA interference have been provided in Table S4. For the differentiation assay, the cells were cultured with 200 ng/ml recombinant human bone morphogenetic protein 2 (rhBMP2, Wako) for 3 days.

Isolation of DRMs

After 2 days of incubation, mDP cells treated with or without MβCD were homogenized in lysis buffer (25 mM Tris-HCl [pH 7.4], 150 mM NaCl, 5 mM EDTA, 5 mM dithiothreitol) supplemented with a 1% protease inhibitor (PI) mixture and 1 mM phenylmethylsulfonyl fluoride (PMSF). The homogenate was then centrifuged at 1000g for 10 min. Subsequently, the supernatant was adjusted with 1% Triton X-100 and incubated on ice for 30 min. Gradients were prepared by mixing 1 ml of the solubilized sample with 2 ml of OptiPrep stock (60%) (1893, SEW) and overlaying with 5 ml of 30% OptiPrep (in lysis buffer+PI+PMSF) and 5 ml of 5% OptiPrep. The gradients were ultracentrifuged at 160,000g for 4 h at 4 °C (HITACHI himac CP80NX; P40ST rotor), after which ten fractions were collected from the top of the gradient. Trichloroacetic acid/acetone precipitation was used for protein purification and processed for Western blotting.

LYPD1 regulates odontoblast differentiation

Ex vivo organ cultures

Tooth germs from mandibular molars dissected from E15 mouse embryos were seeded into cell culture inserts (Corning) and grown using an air–liquid interface culture technique in Dulbecco's modified Eagle's medium/F-12 supplemented with 20% fetal bovine serum, 180 µg/ml ascorbic acid, 2 mM l-glutamine, and 50 U/ml penicillin/streptomycin at 37 °C in a humidified atmosphere of 5% CO₂ for 7 days, as described (57). For siRNA-mediated knockdown, tooth germs were transfected with *Lypd1* siRNA (Dharmacon) or control siRNA (Dharmacon) at a concentration of 500 nM using Lipofectamine 3000 reagent, according to the manufacturer's protocol. To investigate the role of lipid rafts in tooth development, the lipid raft-targeting drugs MβCD (1 mM, Sigma-Aldrich), simvastatin (1 µM, Wako), and fumonisins B1 (40 µM, Wako) were added to the organ culture medium, which was replaced every 2 days. To evaluate tooth differentiation, 7-day cultured E15 tooth germs treated with siRNA or lipid raft-targeting drugs were harvested and the expression of dental mesenchymal differentiation marker genes was examined.

RNA isolation and qRT-PCR analysis

Tissue samples (tooth, brain, eye, colon, heart, kidney, liver, lung, skin, and stomach) were dissected from E16 ICR mouse embryos. Mandibular molar tooth germs were dissected at each developmental stage (E12, E13, E14, E15, E16, E18), P1, P3, and P7. E16 tooth germs were treated with type I collagenase (246 U/ml) at 4 °C for 90 min for separating the epithelium and mesenchyme. Total RNA was extracted from these tissue samples and cultured cells using TRIzol reagent and purified using the RNeasy Mini Kit. Using SuperScript III reverse transcriptase reagent (Invitrogen) and random hexamers (Invitrogen), 2 µg of total RNA was used for synthesizing complementary DNA (cDNA), which was used as a template for qRT-PCR with specific forward and reverse primers listed in Table S5. The expression levels of each gene were normalized to that of *Gapdh*. qRT-PCR reactions were performed using iQ SYBR Green Supermix (Bio-Rad) and the CFX Connect Real-Time PCR detection system (Bio-Rad). The mRNA levels were compared with that of *Gapdh* using the $\Delta\Delta C_t$ method.

Western blot analysis

After being transfected with siRNA or treated with lipid raft-targeting drugs, the total proteins of mDP cells or 7-day cultured E15 tooth germs were dissolved in CelLytic M or CelLytic MT (Sigma-Aldrich) buffers supplemented with a 1% PI mixture and 1 mM PMSE. The lysates were centrifuged at 12,000 rpm for 10 min, and the protein concentration of each sample was measured by the Pierce BCA Protein Assay kit (Thermo Scientific). After denaturation at 70 °C for 10 min, 10 µg of protein from each sample was subjected to 4 to 12% sodium dodecyl sulfate-polyacrylamide gel electrophoresis (NuPAGE, Invitrogen). Subsequently, the proteins were blotted onto a PVDF membrane (Invitrogen) and analyzed by Western blotting. The membranes were blocked with Blocking

One-P (Nacalai Tesque) for 10 min and immunoblotted with antibodies listed in Table S6. The signals were visualized using an ECL kit (Thermo Scientific) and the ImageQuant 800 system (GE Healthcare).

Alkaline phosphatase assay

mDP cells transferred with control siRNA and *Lypd1* siRNA were seeded and cultured for 5 days. On days 1, 3, and 5 after transfection, cell differentiation ability was measured using a TRACP and ALP Assay Kit (Takara Bio). The absorbance at 405 nm for Alp activity was detected using an iMark microplate reader. In addition, Alp staining was performed using the TRACP and ALP double-stain kit (Takara Bio). The cells were washed with PBS, and 5-bromo-4-chloro-3-indolyl phosphate/nitroblue tetrazolium liquid substrate was added to each well, followed by a 25-min incubation in the dark at 37 °C. Alp-positive cells appeared dark purple when visualized under a light microscope. The images were captured using a KEYENCE BZ-X800.

Construction of expression vector

LYPD1 expression vectors were constructed using a Gateway cloning system (Invitrogen) according to the manufacturer's protocol. Briefly, the coding sequences of mouse LYPD1 without a stop codon were cloned into a pENTR/D-TOPO entry vector. cDNA was prepared from E16 brain mRNA by reverse transcription PCR, and the sequences were confirmed by DNA sequencing. The primers listed in Table S4 were used. Expression vectors were cloned *via* an LR recombination reaction between the entry clone and destination vectors (Vivid Colors pcDNA6.2/C-EmGFP-DEST and pcDNA-DEST40, respectively) (Invitrogen) and subsequently tagged with Em-GFP and V5-His, respectively. All EmGFP appearing in this paper were abbreviated to GFP.

Immunofluorescence staining

After 7 days of culture, E15 tooth germs transfected with control and *Lypd1* siRNA were frozen in optimal cutting temperature compound (4583; Sakura) at –80 °C and then cut into frozen sections of 10 µm thickness. mDP cells were transfected with mock-EGFP, LYPD1-FL-EmGFP, and LYPD1-ΔGPI-EmGFP using a Neon Transfection System and subsequently seeded in a 4-well chamber at a density of 8 × 10⁴ cells/well. Frozen sections and mDP cells were fixed with 4% PFA and permeabilized with 0.05% Triton X-100 in PBS. Primary antibody and secondary antibodies are listed in Table S5. The nuclei were visualized using DAPI. The fluorescence signal was captured under a confocal laser scanning microscope (LSM700, Carl Zeiss). The cell size and cellular protrusions of each group were calculated using the ImageJ software (version 1.53a, National Institute of Health).

Flow cytometry and cell sorting

For flow cytometry and cell sorting, 48 h following transfection with LYPD1-FL-EmGFP or LYPD1-ΔGPI-EmGFP, mDP cells were harvested and resuspended in 500 µl of PBS

containing 1% bovine serum albumin (5×10^6 cells/ml). The dissociated cells were subjected to flow cytometry and cell sorting using the FACSaria Fusion (BD Biosciences) with a laser of 488 nm for excitation. Small debris was removed by gating in the forward scatter (FSC)/side scatter (SSC) axis, and the doublets were gated out using the axes of FSC-A/FSC-W and SSC-A/SSC-W. In the experiments, 20,000 events were recorded at a rate of approximately 1000 events per second. During measurement, the collected fluorescence data were visualized using the FACS Diva software (BD Biosciences, ver.8). GFP-expressing cells were sorted from the mDP cell suspensions and immediately subjected to RNA isolation and qRT-PCR. At least 50,000 events were acquired for each sample.

Statistical analysis

Each experiment was repeated at least three times to confirm reproducibility. Statistical analysis for each experiment is described in the figure legends. Differences between two groups of data were analyzed *via* two-tailed unpaired Student's *t* tests. One-way ANOVA analysis of variance and Tukey's multiple-comparison test were used for quantification between multiple groups. All statistical analyses were performed using GraphPad Prism 9.3.1, and *p*-values less than 0.05 were considered to indicate statistical significance.

Data availability

The datasets generated and/or analyzed during the current study are available in the NCBI GEO: GSE206135.

Supporting information—This article contains supporting information.

Acknowledgments—We appreciate the technical assistance from The Research Support Center, Research Center for Human Disease Modeling, Kyushu University Graduate School of Medical Sciences. This work utilized the computational resources of the NIH HPC Biowulf cluster (<http://hpc.nih.gov>). We would like to thank NIDCD/NIDCR Genomics and Computational Biology Core authors: E. T. Boger (National Institute on Deafness and Other Communication Disorders, National Institutes of Health, Bethesda, Maryland, USA); B. Choudhury (National Institute on Deafness and Other Communication Disorders, National Institutes of Health, Bethesda, Maryland, USA); D. Martin (National Institute of Dental and Craniofacial Research, National Institutes of Health, Bethesda, Maryland, USA); C. Zheng (National Institute of Dental and Craniofacial Research, National Institutes of Health, Bethesda, Maryland, USA); Z. Wei (National Institute of Dental and Craniofacial Research, National Institutes of Health, Bethesda, Maryland, USA); R. J. Morell (National Institute on Deafness and Other Communication Disorders, National Institutes of Health, Bethesda, Maryland, USA). We also wish to thank Editage (www.editage.com) for English language editing. This work was supported by funds from the NIDCD, National Institutes of Health Division of Intramural Research (ZIC DC000086 to the G. C. B. C.), NIDCR, National Institutes of Health Transfer Core Facility (ZIC DE000744-04), Veterinary Resources Core (ZIC DE000740-05), and

the combined technical research core facility (ZIC DE000729-09). The content is solely the responsibility of the authors and does not necessarily represent the official views of the National Institutes of Health.

Author contributions—Y. F., K. M., and K. Y. conceptualization; Y. F., K. M., and Y. C. methodology; K. M., Y. C., and K. Y. validation; K. F., T. Y., T. T., K. M., J. K., L. Z., and D. M. formal analysis; Y. F., and K. M. investigation; Y. F., K. M., and Y. C. data curation; Y. F. and K. M. writing—original draft; Y. C., K. Y., and I. T. writing—review & editing; T. I., I. T., S. F., and K. Y. supervision; S. F., and K. Y. project administration; S. F. and K. Y. funding acquisition.

Funding and additional information—This study was supported by a Grant-in-Aid from the Japan Society for the Promotion of Science (JSPS) KAKENHI (JP18H03012, JP21K19610, JP21H03150 to K. Y., JP17H01606 to S. F., and JP20K18786 to K. M.), JST FOREST Program (JPMJFR2013 to K. Y.), and JST SPRING (Grant Number JPMJSP2136). K. Y. was supported by Takeda Science Foundation. Y. F. was supported by an Otsuka-Toshimi Scholarship.

Conflict of interest—The authors declare that they have no conflicts of interest with the contents of this article.

Abbreviations—The abbreviations used are: ALPL, alkaline phosphatase; BMP, bone morphogenetic protein; DEG, differentially expressed gene; DMSC, dental mesenchymal stem cell; DPCs, dental papilla cells; DRMs, detergent-resistant membranes; DSPP, dentin sialophosphoprotein; FSC, forward scatter; GPI-APs, glycosylphosphatidylinositol-anchored proteins; ISH, *in situ* hybridization; LYPD1, lymphocyte antigen-6 (Ly6)/Plaur domain-containing 1; M β CD, methyl- β -cyclodextrin; mDP, mouse dental pulp; PANX3, pannexin 3; PI, protease inhibitor; qRT-PCR, real-time quantitative RT-PCR; scRNA-seq, single-cell RNA sequencing; SSC, side scatter.

References

1. Simons, K., and Ikonen, E. (1997) Functional rafts in cell membranes. *Nature* **387**, 569–572
2. Sezgin, E., Levental, I., Mayor, S., and Eggeling, C. (2017) The mystery of membrane organization: composition, regulation and roles of lipid rafts. *Nat. Rev. Mol. Cell Biol.* **18**, 361–374
3. Simons, K., and Ehehalt, R. (2002) Cholesterol, lipid rafts, and disease. *J. Clin. Invest.* **110**, 597–603
4. Hryniewicz-Jankowska, A., Augoff, K., Biernatowska, A., Podkalicka, J., and Sikorski, A. F. (2014) Membrane rafts as a novel target in cancer therapy. *Biochim. Biophys. Acta* **1845**, 155–165
5. Bieberich, E. (2012) It's a lipid's world: bioactive lipid metabolism and signaling in neural stem cell differentiation. *Neurochem. Res.* **37**, 1208–1229
6. Mattei, V., Santacrose, C., Tasciotti, V., Martellucci, S., Santilli, F., Manganelli, V., *et al.* (2015) Role of lipid rafts in neuronal differentiation of dental pulp-derived stem cells. *Exp. Cell Res.* **339**, 231–240
7. Khavandgar, Z., Alebrahim, S., Eimar, H., Tamimi, F., McKee, M. D., and Murshed, M. (2013) Local regulation of tooth mineralization by sphingomyelin phosphodiesterase 3. *J. Dent. Res.* **92**, 358–364
8. Matsuzaka, Y., Tanihata, J., Ooshima, Y., Yamada, D., Sekiguchi, M., Miyatake, S., *et al.* (2020) The nSMase2/Smpd3 gene modulates the severity of muscular dystrophy and the emotional stress response in mdx mice. *BMC Med.* **18**, 343
9. Seppala, M., Thivichon-Prince, B., Xavier, G. M., Shaffie, N., Sangani, I., Birjandi, A. A., *et al.* (2022) Gas1 regulates patterning of the murine and human dentitions through sonic hedgehog. *J. Dent. Res.* **101**, 473–482

LYPD1 regulates odontoblast differentiation

- Kinoshita, T. (2020) Biosynthesis and biology of mammalian GPI-anchored proteins. *Open Biol.* **10**, 190290
- Munro, S. (2003) Lipid rafts: elusive or illusive? *Cell* **115**, 377–388
- Thesleff, I., and Sharpe, P. (1997) Signalling networks regulating dental development. *Mech. Dev.* **67**, 111–123
- Mina, M., and Kollar, E. J. (1987) The induction of odontogenesis in non-dental mesenchyme combined with early murine mandibular arch epithelium. *Arch. Oral Biol.* **32**, 123–127
- Kollar, E. J., and Baird, G. R. (1969) The influence of the dental papilla on the development of tooth shape in embryonic mouse tooth germs. *J. Embryol. Exp. Morphol.* **21**, 131–148
- Iwamoto, T., Nakamura, T., Ishikawa, M., Yoshizaki, K., Sugimoto, A., Ida-Yonemochi, H., et al. (2017) Pannexin 3 regulates proliferation and differentiation of odontoblasts via its hemichannel activities. *PLoS One* **12**, e0177557
- Shiba, H. (2003) Enhancement of alkaline phosphatase synthesis in pulp cells co-cultured with epithelial cells derived from lower rabbit incisors. *Cell Biol. Int.* **27**, 815–823
- Sreenath, T., Thyagarajan, T., Hall, B., Longenecker, G., D'Souza, R., Hong, S., et al. (2003) Dentin sialophosphoprotein knockout mouse teeth display widened predentin zone and develop defective dentin mineralization similar to human dentinogenesis imperfecta type III. *J. Biol. Chem.* **278**, 24874–24880
- Kettunen, P., Laurikkala, J., Itäranta, P., Vainio, S., Itoh, N., and Thesleff, I. (2000) Associations of FGF-3 and FGF-10 with signaling networks regulating tooth morphogenesis. *Dev. Dyn.* **219**, 322–332
- Trapnell, C., Cacchiarelli, D., Grimsby, J., Pokharel, P., Li, S., Morse, M., et al. (2014) The dynamics and regulators of cell fate decisions are revealed by pseudotemporal ordering of single cells. *Nat. Biotechnol.* **32**, 381–386
- Friedrichson, T., and Kurzchalia, T. V. (1998) Microdomains of GPI-anchored proteins in living cells revealed by crosslinking. *Nature* **394**, 802–805
- Gaus, K., Rodriguez, M., Ruberu, K. R., Gelissen, I., Sloane, T. M., Kriharides, L., et al. (2005) Domain-specific lipid distribution in macrophage plasma membranes. *J. Lipid Res.* **46**, 1526–1538
- Yokose, S., and Naka, T. (2010) Lymphocyte enhancer-binding factor 1: an essential factor in odontoblastic differentiation of dental pulp cells enzymatically isolated from rat incisors. *J. Bone Miner. Metab.* **28**, 650–658
- Kajiura, K., Umemura, N., Ohkoshi, E., Ohta, T., Kondoh, N., and Kawano, S. (2021) Shikonin induces odontoblastic differentiation of dental pulp stem cells via AKT-mTOR signaling in the presence of CD44. *Connect. Tissue Res.* **62**, 689–697
- Cho, Y. D., Yoon, W. J., Woo, K. M., Baek, J. H., Park, J. C., and Ryoo, H. M. (2010) The canonical BMP signaling pathway plays a crucial part in stimulation of dentin sialophosphoprotein expression by BMP-2. *J. Biol. Chem.* **285**, 36369–36376
- Hollnagel, A., Oehlmann, V., Heymer, J., Rütter, U., and Nordheim, A. (1999) Id genes are direct targets of bone morphogenetic protein induction in embryonic stem cells. *J. Biol. Chem.* **274**, 19838–19845
- Yang, W., Harris, M. A., Cui, Y., Mishina, Y., Harris, S. E., and Gluhak-Heinrich, J. (2012) Bmp2 is required for odontoblast differentiation and pulp vasculogenesis. *J. Dent. Res.* **91**, 58–64
- Bizet, A. A., Liu, K., Tran-Khanh, N., Saksena, A., Vorstenbosch, J., Finnson, K. W., et al. (2011) The TGF-beta co-receptor, CD109, promotes internalization and degradation of TGF-beta receptors. *Biochim. Biophys. Acta* **1813**, 742–753
- Tsui, C. C., Gabreski, N. A., Hein, S. J., and Pierchala, B. A. (2015) Lipid rafts are physiologic membrane microdomains necessary for the morphogenic and developmental functions of glial cell line-derived neurotrophic factor in vivo. *J. Neurosci.* **35**, 13233–13243
- Özhan, G., Sezgin, E., Wehner, D., Pfister, A. S., Kuhl, S. J., Kagermeier-Schenk, B., et al. (2013) Lypd6 enhances Wnt/beta-catenin signaling by promoting Lrp6 phosphorylation in raft plasma membrane domains. *Dev. Cell* **26**, 331–345
- Samad, T. A., Rebbapragada, A., Bell, E., Zhang, Y., Sidis, Y., Jeong, S. J., et al. (2005) DRAGON, a bone morphogenetic protein co-receptor. *J. Biol. Chem.* **280**, 14122–14129
- Saitoh, S., Kosugi, A., Noda, S., Yamamoto, N., Ogata, M., Minami, Y., et al. (1995) Modulation of TCR-mediated signaling pathway by thymic shared antigen-1 (TSA-1)/stem cell antigen-2 (Sca-2). *J. Immunol.* **155**, 5574–5581
- Kim, N. C., and Marqués, G. (2012) The Ly6 neurotoxin-like molecule target of wit regulates spontaneous neurotransmitter release at the developing neuromuscular junction in *Drosophila*. *Dev. Neurobiol.* **72**, 1541–1558
- Loughner, C. L., Bruford, E. A., McAndrews, M. S., Delp, E. E., Swamy-nathan, S., and Swamynathan, S. K. (2016) Organization, evolution and functions of the human and mouse Ly6/uPAR family genes. *Hum. Genomics* **10**, 10
- Lingwood, D., and Simons, K. (2007) Detergent resistance as a tool in membrane research. *Nat. Protoc.* **2**, 2159–2165
- Magee, A. I., and Parmryd, I. (2003) Detergent-resistant membranes and the protein composition of lipid rafts. *Genome Biol.* **4**, 234
- Fujihara, Y., Noda, T., Kobayashi, K., Oji, A., Kobayashi, S., Matsumura, T., et al. (2019) Identification of multiple male reproductive tract-specific proteins that regulate sperm migration through the oviduct in mice. *Proc. Natl. Acad. Sci. U. S. A.* **116**, 18498–18506
- Okumura, R., Kurakawa, T., Nakano, T., Kayama, H., Kinoshita, M., Motooka, D., et al. (2016) Lypd8 promotes the segregation of flagellated microbiota and colonic epithelia. *Nature* **532**, 117–121
- Ilangumaran, S., and Hoessli, D. C. (1998) Effects of cholesterol depletion by cyclodextrin on the sphingolipid microdomains of the plasma membrane. *Biochem. J.* **335**, 433–440
- Alberts, A. W. (1990) Lovastatin and simvastatin—inhibitors of HMG CoA reductase and cholesterol biosynthesis. *Cardiology* **77** Suppl 4, 14–21
- Merrill, A. H., Jr., van Echten, G., Wang, E., and Sandhoff, K. (1993) Fumonisin B1 inhibits sphingosine (sphinganine) N-acyltransferase and de novo sphingolipid biosynthesis in cultured neurons *in situ*. *J. Biol. Chem.* **268**, 27299–27306
- Brusselmans, K., Timmermans, L., Van de Sande, T., Van Veldhoven, P. P., Guan, G., Shechter, I., et al. (2007) Squalene synthase, a determinant of Raft-associated cholesterol and modulator of cancer cell proliferation. *J. Biol. Chem.* **282**, 18777–18785
- Hojjati, M. R., Li, Z., Zhou, H., Tang, S., Huan, C., Ooi, E., et al. (2005) Effect of myricin on plasma sphingolipid metabolism and atherosclerosis in apoE-deficient mice. *J. Biol. Chem.* **280**, 10284–10289
- Miyazaki, K., Yoshizaki, K., Arai, C., Yamada, A., Saito, K., Ishikawa, M., et al. (2016) Plakophilin-1, a novel wnt signaling regulator, is critical for tooth development and ameloblast differentiation. *PLoS One* **11**, e0152206
- Arai, C., Yoshizaki, K., Miyazaki, K., Saito, K., Yamada, A., Han, X., et al. (2017) Nephronectin plays critical roles in Sox2 expression and proliferation in dental epithelial stem cells via EGF-like repeat domains. *Sci. Rep.* **7**, 45181
- Han, X., Yoshizaki, K., Miyazaki, K., Arai, C., Funada, K., Yuta, T., et al. (2018) The transcription factor NKX2-3 mediates p21 expression and ectodysplasin-A signaling in the enamel knot for cusp formation in tooth development. *J. Biol. Chem.* **293**, 14572–14584
- Funada, K., Yoshizaki, K., Miyazaki, K., Han, X., Yuta, T., Tian, T., et al. (2020) microRNA-875-5p plays critical role for mesenchymal condensation in epithelial-mesenchymal interaction during tooth development. *Sci. Rep.* **10**, 4918
- Chiba, Y., Yoshizaki, K., Tian, T., Miyazaki, K., Martin, D., Genomics, et al. (2021) Integration of single-cell RNA- and CAGE-seq reveals tooth-enriched genes. *J. Dent. Res.* **101**, 220345211049785
- Sharir, A., Marangoni, P., Zilionis, R., Wan, M., Wald, T., Hu, J. K., et al. (2019) A large pool of actively cycling progenitors orchestrates self-renewal and injury repair of an ectodermal appendage. *Nat. Cell Biol.* **21**, 1102–1112
- Chiba, Y., Saito, K., Martin, D., Boger, E. T., Rhodes, C., Yoshizaki, K., et al. (2020) Single-cell RNA-sequencing from mouse incisor reveals dental epithelial cell-type specific genes. *Front. Cell Dev. Biol.* **8**, 841

50. Krivanek, J., Soldatov, R. A., Kastriti, M. E., Chontorotzea, T., Herdina, A. N., Petersen, J., *et al.* (2020) Dental cell type atlas reveals stem and differentiated cell types in mouse and human teeth. *Nat. Commun.* **11**, 4816
51. Chen, S., Gluhak-Heinrich, J., Martinez, M., Li, T., Wu, Y., Chuang, H. H., *et al.* (2008) Bone morphogenetic protein 2 mediates dentin sialophosphoprotein expression and odontoblast differentiation via NF- κ B signaling. *J. Biol. Chem.* **283**, 19359–19370
52. Yang, G., Yuan, G., MacDougall, M., Zhi, C., and Chen, S. (2017) BMP-2 induced Dspp transcription is mediated by Dlx3/Osx signaling pathway in odontoblasts. *Sci. Rep.* **7**, 10775
53. Miyazono, K., Kamiya, Y., and Morikawa, M. (2010) Bone morphogenetic protein receptors and signal transduction. *J. Biochem.* **147**, 35–51
54. Narayanan, K., Srinivas, R., Ramachandran, A., Hao, J., Quinn, B., and George, A. (2001) Differentiation of embryonic mesenchymal cells to odontoblast-like cells by overexpression of dentin matrix protein 1. *Proc. Natl. Acad. Sci. U. S. A.* **98**, 4516–4521
55. Wang, X., Chiba, Y., Jia, L., Yoshizaki, K., Saito, K., Yamada, A., *et al.* (2020) Expression patterns of claudin family members during tooth development and the role of Claudin-10 (Cldn10) in cytodifferentiation of stratum intermedium. *Front. Cell Dev. Biol.* **8**, 595593
56. Zheng, G. X., Terry, J. M., Belgrader, P., Ryvkin, P., Bent, Z. W., Wilson, R., *et al.* (2017) Massively parallel digital transcriptional profiling of single cells. *Nat. Commun.* **8**, 14049
57. Han, X., Yoshizaki, K., Tian, T., Miyazaki, K., Takahashi, I., and Fukumoto, S. (2020) Mouse embryonic tooth germ dissection and ex vivo culture protocol. *Bio Protoc.* **10**, e3515